Fast Multi-Objective Antenna Design by ANN-Based Machine Learning with Gradient-Based Design Enhancement

Slawomir Koziel[1,2][0000-0002-9063-2647] and Anna Pietrenko-Dabrowska[2][0000-0003-2319-6782]

[1] Engineering Optimization & Modeling Center, Department of Engineering, Reykjavík University, Menntavegur 1, 102 Reykjavík, Iceland
koziel@ru.is

[2] Faculty of Electronics Telecommunications and Informatics, Gdansk University of Technology, Narutowicza 11/12, 80-233 Gdansk, Poland
anna.dabrowska@pg.edu.pl

Abstract. This research proposes a novel methodology for rapid multi-objective (MO) electromagnetic (EM)-driven design of antenna systems. Our approach integrates machine learning (ML) with neural network metamodels. At each iteration, the surrogate, optimized using an MO-oriented evolutionary algorithm, generates multiple candidate Pareto-optimal designs. These solutions are further refined locally using approximate response Jacobians estimated from the surrogate model. The metamodel itself is continuously updated with EM data collected during the optimization process. By combining surrogate-driven exploration with gradient-based refinement, the method accelerates convergence and enables more accurate identification of Pareto fronts compared to conventional techniques. The framework has been validated on two planar antennas, showcasing excellent cost efficiency: the mean MO expenses are under 300 EM simulations, corresponding to roughly 80% savings relative to offline surrogate-assisted optimization, and substantial speedup over baseline ML methods lacking gradient enhancements. Moreover, the proposed technique produces high-quality Pareto fronts in terms of both distribution uniformity and solution quality, as confirmed by dominance-based performance metrics.

Keywords: Antenna engineering, multi-objective optimization, machine learning, gradient-based tuning, neural networks.

1 Introduction

Modern antennas are required to meet increasingly strict performance demands across a wide range of application areas [1], [2], while simultaneously supporting diverse functionalities [3], [4] and adhering to strict size constraints [5]. Fulfilling these demands often necessitates geometrically complex designs that incorporate advanced components such as metamaterials, defected ground structures, or substrate-integrated waveguides [6], [7]. Achieving optimal performance in such devices calls for precise adjustment of antenna dimensions [8], which, to ensure reliability, must

ICCS Camera Ready Version 2026
To cite this paper please use the final published version:
DOI: 10.1007/978-3-032-29921-5_25

be performed using full-wave electromagnetic (EM) simulations—a computationally expensive process [9]. An additional challenge arises from the need to handle multiple, frequently conflicting objectives [10]. Miniaturization exemplifies this issue, as reducing antenna size typically degrades electrical performance metrics such as reflection response, gain, and robustness to fabrication tolerances [11]. Consequently, practical antenna design involves a careful balance among competing requirements. Identifying feasible trade-offs between these objectives naturally calls for multi-objective optimization (MO) [12].

Managing multiple design variables, objectives, and constraints is only feasible through rigorous optimization techniques [13]. Yet, most existing algorithms are tailored for scalar objectives [14], and their extension to multi-objective (MO) problems often relies on objective aggregation or prioritization [15]. To capture the full spectrum of trade-offs, genuine MO is required, which today is almost exclusively pursued using bio-inspired algorithms [16], [17]. However, direct application of these methods to EM-driven MO is impractical due to their prohibitive computational cost. A viable alternative is surrogate-assisted optimization [18], where inexpensive metamodels are used to approximate antenna responses and thus replace most of the costly EM evaluations. Commonly employed surrogates include radial basis functions, Gaussian process regression, and artificial neural networks [19]–[21]. These models may be constructed offline or iteratively refined within a machine learning (ML) framework [22]. In this setting, candidate solutions (infill points) are generated according to various criteria, such as accuracy improvement, global optimum identification, or balanced exploration and exploitation [23]. Nonetheless, ML-based approaches face two key challenges. First, the search process tends to concentrate too quickly on a specific region, leaving other areas of the design space underexplored. Second, constructing reliable surrogates is inherently difficult due to the dimensionality-related issues and the large spatial extent of typical design spaces. These limitations can be alleviated through domain confinement. One strategy is to define the search region using non-dominated solutions obtained by optimizing individual objectives [24]. Another is performance-driven modeling [25], which restricts the domain to regions containing high-quality designs. Such confinement significantly boosts predictive accuracy [26]. While successfully applied to MO [27], this approach incurs considerable upfront costs, as it requires identifying extreme non-dominated solutions through supplementary optimization runs.

This research introduces a new methodology for EM-driven multi-objective optimization (MO) of antennas. The proposed framework integrates artificial neural network (ANN) surrogates within a machine learning (ML) scheme. At each step, several infill designs are produced by optimizing the surrogate. These candidate designs are further refined through local gradient-based corrections realized through a trust-region framework, with sensitivities estimated directly from the ANN model. The EM data gathered during the process is used to adaptively improve the surrogate, ensuring accuracy throughout the search. By interleaving ML-based predictions with local refinement, the method achieves both faster convergence and higher-quality Pareto sets. The approach is extensively verified using two planar antennas optimized for best reflection response, miniaturization, and gain enhancement. The results underscore competitive cost efficiency and robustness in comparison to several benchmarks. The typical computational

ICCS Camera Ready Version 2026
To cite this paper please use the final published version:
DOI: 10.1007/978-3-032-29921-5_25

burden does not exceed 300 EM simulations, corresponding to about 80% savings relative to offline surrogate-assisted methods and a 20% acceleration over ML frameworks without gradient-based refinement.

2 Multi-Objective Optimization by Machine Learning with Local Design Enhancement

This part of the paper explains the details proposed MO framework. In Section 2.1 we discuss the MO problem formulation. ANN surrogate model and multi-objective evolutionary algorithms are outlined in Sections 2.2 and 2.3, respectively. The proposed ML procedure is elucidated in Section 2.4, whereas Section 2.5 covers local gradient-based solution enhancement. Training dataset updating rules are elaborated on in Section 2.6. The complete algorithm is summarized in Section 2.7.

2.1 Problem Formulation

The aim of MO is to identify the Pareto set. The latter is a finite subset of the Pareto front [28], representing the best available compromise designs given the considered design objectives. The necessary notation is presented in Fig. 1. Nowadays, MO is most often realized using bio-inspired techniques [29]. These methods can generate the entire Pareto set within a single algorithm run. Notwithstanding, they are extremely expensive. Practical alternatives are machine learning (ML) methods [30], [31], but the challenges associated with the construction of reliable behavioral models impede ML efficacy in more complex tasks. The methodology presented in this study attempts to mitigate these difficulties by combining ML with multiple candidate solution renditions and local gradient-based design enhancement. The latter is interleaved with the ML iterations. The details of our strategy are provided in the next sub-sections.

2.2 Surrogate Model

The MO algorithm proposed here employs an artificial neural network (ANN) surrogate, specifically a multi-layer perceptron (MLP) [32], configured as follows: (i) two hidden layers, (ii) ten neurons per layer, (iii) sigmoid activation functions, and (iv) hyperparameter training using the Levenberg–Marquardt backpropagation algorithm, with 1000 learning epochs.

Symbol	Explanation
$\boldsymbol{x} = [x_1 \ldots x_n]^T$	Vector of design variables
X	Parameter space defined by the lower and upper bounds on variables $\boldsymbol{x}$, $\boldsymbol{l} = [l_1 \ldots l_n]^T$ and $\boldsymbol{u} = [u_1 \ldots u_n]^T$
$\boldsymbol{F}(\boldsymbol{x}) = [F_1(\boldsymbol{x}) \ldots F_{Nobj}(\boldsymbol{x})]^T$	Design goals (all to be minimized); N_{obj} is the number of objectives
$\boldsymbol{R}(\boldsymbol{x})$	Response of the EM simulation model (e.g., $\lvert S_{11}\rvert$ versus frequency)
$\prec$	Pareto dominance relation: design $\boldsymbol{x}$ dominates over the design $\boldsymbol{y}$ (or, $\boldsymbol{x} \prec \boldsymbol{y}$) if $F_k(\boldsymbol{x}) \leq F_k(\boldsymbol{y})$ for all $k = 1, \ldots, N_{obj}$, and $F_k(\boldsymbol{x}) < F_k(\boldsymbol{y})$ for at least one k
X_P	Pareto front: the set of globally non-dominated designs $\boldsymbol{x} \in X$ in the sense of relation $\prec$, i.e., $\boldsymbol{x} \in X_P$ if and only if for any $\boldsymbol{y} \in X$, $\boldsymbol{x}$ is not dominated by $\boldsymbol{y}$

Fig. 1. Antenna MO: notation.

ICCS Camera Ready Version 2026
To cite this paper please use the final published version:
DOI: 10.1007/978-3-032-29921-5_25

Model performance is assessed via mean square error (MSE). The available data is randomly split into training and testing subsets. This architecture was selected based on preliminary experiments. The inputs of the model are design parameters $\boldsymbol{x}$. The model's outputs are frequency responses, specifically reflection coefficient S_{11} and realized gain. For complex-valued responses, individual models are constructed for the real and imaginary components, as shown in Fig. 2. Owing to its architectural simplicity, ANN training is computationally efficient, typically requiring only a few seconds, which is negligible compared to the EM analysis-related expenses. The initial training dataset, $\boldsymbol{x}_B^{(j)}$, $j = 1, \ldots, N_{init}$, is generated with the help of a Latin Hypercube Sampling (LHS) scheme [33]. The training set is subsequently enriched with infill points produced by the machine learning process.

2.3 Multi-Objective Evolutionary Algorithm

The fundamental step in the ML-based antenna optimization process is to generate the (candidate) Pareto set by optimizing the surrogate model. Here, it is realized using a standard multi-objective evolutionary algorithm (MOEA) [34]. The MOEA routine uses floating-point representation, Pareto ranking for candidate solution assessment, fitness sharing with adaptive niche size, and mating restrictions to avoid clustering, as well as Pareto-ranking-based tournament selection. Here is the algorithm setup: population size $N_P = 200$, crossover and mutation rates $p_m = 0.8$ and $p_c = 0.1$ (see [34] for more details). As the algorithm operates on the data-driven metamodel, its running cost is negligible.

2.4 Infill Point Generation by Machine Learning

The ML procedure yields N_{infill} candidate solutions $\boldsymbol{x}_I^{(i,j)}$, $j = 1, \ldots, N_{infill}$ per iteration, where i stands for the iteration counter. These points are selected from the current approximation of the Pareto set produced by optimizing the ANN metamodel (cf. Section 2.3). The selection process is visualized in Fig. 3. We aim to yield an equidistant Pareto front coverage. Therefore, the candidate solutions are selected to be near the target levels F_j within the current range of the second design goal F_2. The range is assessed using the actual spread of the current Pareto front, and optional acceptance thresholds for the first objective (e.g., –10 dB for $|S_{11}|$). We set $F_j = F_{2.\min} + (F_{2.\max} - F_{2.\min})(j-1)/(N_{\text{infill}} - 1)$. The new parameter vectors are then inserted into the training set.

Because of the limited predictive accuracy of the surrogate, design objectives assessed through EM simulations are generally inferior to those predicted by the metamodel. Consequently, the surrogate serves only as an auxiliary tool within the MO process, while EM-evaluated data points remain the sole basis for decision-making. In particular, both the Pareto set quality and the stopping criteria are determined exclusively from EM results.

2.5 Local Solution Enhancement

To improve the efficacy of the MO process, it is essential to guide candidate solutions toward the Pareto front as rapidly as possible. In this work, we introduce an additional step—gradient-based design refinement—applied to every solution generated by the ML process. Antenna response gradients are estimated using the ANN surrogate at negligible cost. Moreover, as the surrogate gains reliability in the parameter space region surrounding the Pareto front, the accuracy of sensitivity estimation improves accordingly. The local refinement procedure is detailed below.

ICCS Camera Ready Version 2026
To cite this paper please use the final published version:
DOI: 10.1007/978-3-032-29921-5_25

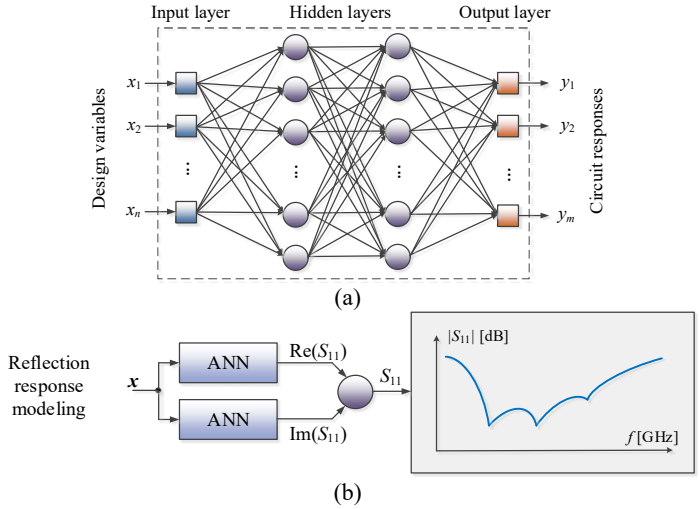

Fig. 2. The ANN surrogate used by the proposed MO framework: (a) ANN architecture, (b) modelling of complex-valued responses; for the reflection response, the real and imaginary parts are modelled individually. The model's inputs are antenna parameters $\boldsymbol{x}$; the outputs are electrical characteristics at discrete frequencies f_1 through f_m.

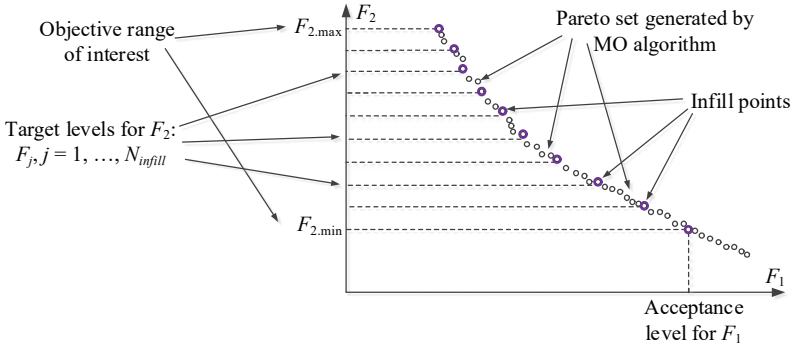

Fig. 3. Infill point generation. The infill vectors are identified from the Pareto set obtained through ANN metamodel optimization. The selection criterion is to achieve equidistant distribution regarding objective F_2; its range is established based on the current Pareto front spread. The target levels F_j are set as $F_j = F_{2.\min} + (F_{2.\max} - F_{2.\min})(j-1)/(N_{\text{infill}}-1)$.

We denote by $\boldsymbol{R}(\boldsymbol{x}_I^{(i,j)})$ and $\boldsymbol{R}_S(\boldsymbol{x}_I^{(i,j)})$ the EM- and surrogate-evaluated antenna responses at the candidate solution $\boldsymbol{x}_I^{(i,j)}$, respectively, and by $\boldsymbol{J}_S(\boldsymbol{x}_I^{(i,j)})$ the Jacobian computed with the help of the ANN model. Using this data, we build an auxiliary model

$$\boldsymbol{L}^{(i,j)}(\boldsymbol{x}) = \boldsymbol{R}(\boldsymbol{x}_I^{(i,j)}) + \boldsymbol{J}_S(\boldsymbol{x}_I^{(i,j)}) \cdot (\boldsymbol{x} - \boldsymbol{x}_I^{(i,j)}) \quad (1)$$

and obtain an enhanced solution as

$$\boldsymbol{x}_G^{(i,j)} = \arg \min_{\boldsymbol{x}, \|\boldsymbol{x}-\boldsymbol{x}_I^{(i,j)}\| \le d^{(i,j)}} F_{1.L}(\boldsymbol{x}) \quad (2)$$

In (2), $F_{1.L}(\boldsymbol{x})$ is the first objective evaluated using (1). Solving (2) is subject to

ICCS Camera Ready Version 2026
To cite this paper please use the final published version:
DOI: 10.1007/978-3-032-29921-5_25

$$F_{k.L}(\boldsymbol{x}) \le F_{k.L}(\boldsymbol{x}_I^{(i.j)}), \quad k = 2, ..., N_{obj} \tag{3}$$

where $F_{k.L}(\boldsymbol{x})$ are the respective objectives evaluated using the model (1). Extra conditions are considered to ensure that enhancing the first design goal does not degrade the others. This approach results in relocating the parameter vectors towards the Pareto front. The search region $d^{(i,j)}$ is updated for each point using the standard trust-region (TR) rules [35]. For that, we compute a gain ratio

$$r = \frac{F_1(\boldsymbol{x}_G^{(i.j)}) - F_1(\boldsymbol{x}_I^{(i.j)})}{F_{1.L}(\boldsymbol{x}_G^{(i.j)}) - F_{1.L}(\boldsymbol{x}_I^{(i.j)})}, \quad j = 1, \ldots, N_{infill} \tag{4}$$

If $r > 0.75$, we set $d^{(i+1,j)} = 1.5d^{(i,j)}$, else, if $r < 0.25$ $d^{(i+1,j)} = d^{(i,j)}/2$.

The enhanced point $\boldsymbol{x}_G^{(i,j)}$ is found by executing a single TR iteration, the cost of which is just a single EM analysis. All vectors $\boldsymbol{x}_G^{(i,j)}$ are incorporated into the overall training dataset as all new samples provide invaluable information for subsequent iterations of the ML algorithm.

2.6 Training Dataset Updates. ML Iteration. Termination Conditions

As mentioned, the infill vectors are inserted into the training set along with the gradient-enhanced points discussed in Section 2.5. Let $\boldsymbol{x}_T^{(i-1,j)}$, $j = 1, \ldots, N_T$, be the training set at the ith MO iteration, and $\boldsymbol{R}(\boldsymbol{x}_T^{(i-1,j)})$ be the corresponding EM-simulated antenna responses. Upon initial sampling, $N_T = N_{init}$, $\boldsymbol{x}_T^{(0,j)} = \boldsymbol{x}_B^{(j)}$, $j = 1, \ldots, N_T$. Further, let $\boldsymbol{x}_I^{(i,j)}$, $j = 1, \ldots, N_{infill}$, be candidate solutions obtained in the ith iteration, whereas $\boldsymbol{x}_G^{(i,j)}$, $j = 1, \ldots, N_{infill}$, be locally-tuned points. The updated dataset is constructed by incorporating the infill points into $\{\boldsymbol{x}_T^{(i,j)}\} = \{\boldsymbol{x}_T^{(i-1,j)}\} \cup \{\boldsymbol{x}_I^{(i,j)}\} \cup \{\boldsymbol{x}_G^{(i,j)}\}$. Figure 4 shows a flow diagram of a single ML iteration, representing ANN model rendition, Pareto set rendition, infill point extraction and enhancement, and training dataset updating.

The stopping criteria are based on the convergence of the Pareto set representation evaluated through EM analysis. The convergence metric involves the comparison of the ML-generated infill points in the ith iteration, $\{\boldsymbol{x}_I^{(i,j)}\}$, and their enhanced versions $\{\boldsymbol{x}_G^{(i,j)}\}$. We define

$$E_i = \left\| \boldsymbol{X}_I^{(i)} - \boldsymbol{X}_G^{(i)} \right\| \tag{5}$$

where $\boldsymbol{X}_I^{(i)}$ and $\boldsymbol{X}_G^{(i)}$ are $n \times N_{infill}$ matrices

$$\boldsymbol{X}_I^{(i)} = \left[\boldsymbol{x}_I^{(i.1)} \ldots \boldsymbol{x}_I^{(i.N_{infill})} \right] \tag{6}$$

$$\boldsymbol{X}_G^{(i)} = \left[\boldsymbol{x}_G^{(i.1)} \ldots \boldsymbol{x}_G^{(i.N_{infill})} \right] \tag{7}$$

Upon convergence, E_i gradually decreases. However, because of a partially stochastic nature of the search process, large fluctuations of E_i are possible at individual iterations. To improve stability, a moving average $E_{a.i}$ is employed, defined as

$$E_{a.i} = \frac{1}{i - \max\{1, i - N_a + 1\} + 1} \sum_{k=\max\{1, i-N_a+1\}}^{i} E_k \tag{8}$$

The termination criterion based on (8) takes the form of

$$E_{a.i} < \varepsilon \tag{9}$$

where ε is the convergence threshold.

ICCS Camera Ready Version 2026
To cite this paper please use the final published version:
DOI: 10.1007/978-3-032-29921-5_25

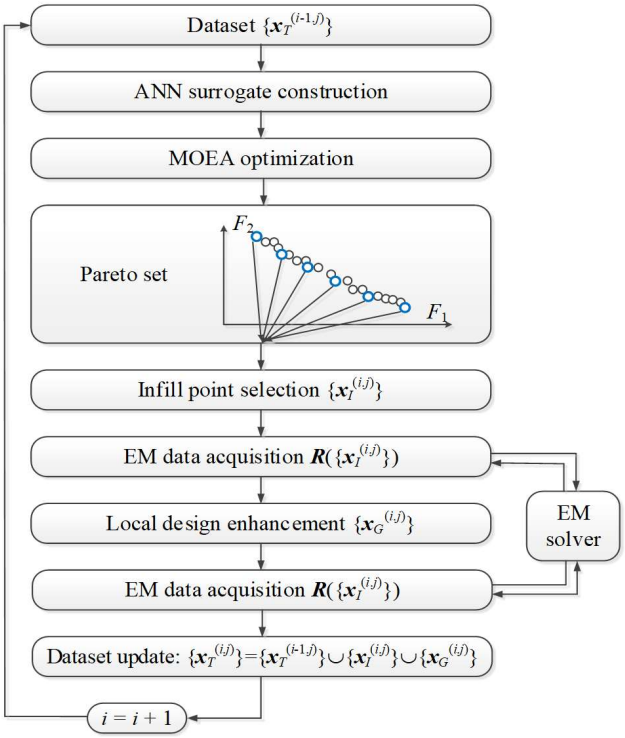

Fig. 4. Flow diagram of a single ML iteration. Surrogate built using the dataset $\{x_T^{(i-1,j)}\}$ is optimized by MOEA. New candidate designs obtained from the Pareto set are locally enhanced (cf. (1)-(3)). The EM simulation data collected during the iteration expands the training dataset.

2.7 Complete Algorithm

The block diagram of the presented MO algorithm is illustrated in Fig. 5. There are several key stages: initial sampling and EM data collection, surrogate model construction, and the ML-driven search. The latter involves approximating the Pareto set using MOEA, extracting infill points, and applying local refinement. Incorporating both infill and refined solutions into the training set accelerates the search by steering candidate designs closer to the genuine Pareto front. Simultaneously, the growing amount of samples in the front region enhances the accuracy of the ANN surrogate, which further supports faster convergence.

The procedure's control parameters are summarized in Table 1. Only a few parameters are required, mainly related to dataset sizes and termination criteria. In the verification experiments of Section 3, the default values listed in the last column of Table 1 are used. Details of the MOEA and ANN settings are provided in Sections 2.2 and 2.3. Since the majority of operations are performed using the surrogate, the actual optimization cost is largely dictated by the overall number of EM analyses executed during the algorithm run.

ICCS Camera Ready Version 2026
To cite this paper please use the final published version:
DOI: 10.1007/978-3-032-29921-5_25

Table 1. Control parameters

Parameter	Description	Default value
N_{init}	The number of initial sample points for constructing the first ANN surrogate	100
N_{infill}	The number of infill points generated per MO iteration	10
N_a	The span of the moving average for computing the similarity metric $E_{a,i}$	5
ε	Termination threshold for the MO process	1

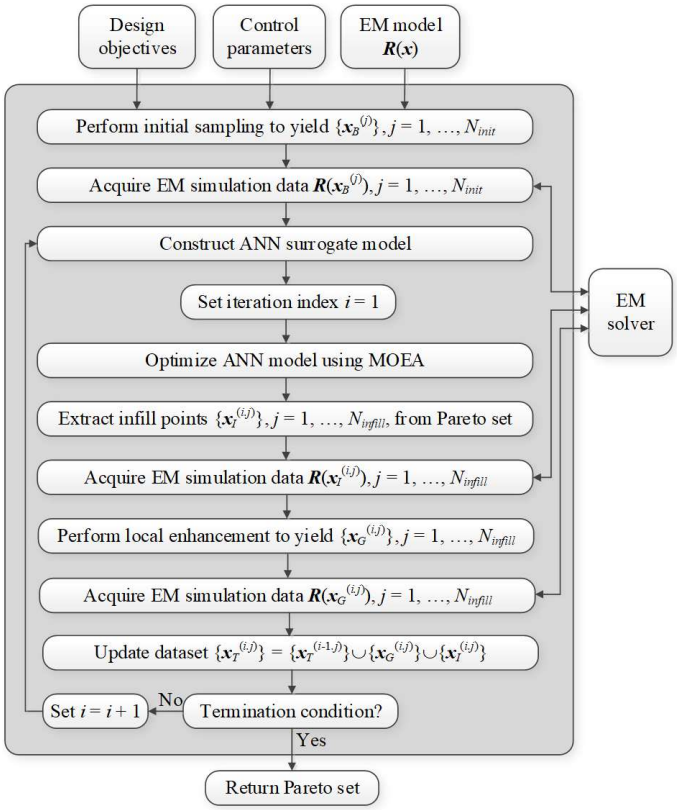

Fig. 5. Block diagram of the suggested MO framework.

3 Results

Here, we showcase the performance of our MO algorithm using two microstrip antennas: a broadband monopole optimized for best reflection response and minimum size, and a quasi-Yagi structure designed for best impedance matching and end-fire gain enhancement. Our technique is benchmarked against several surrogate-assisted MO benchmark procedures. We compare the cost efficiency and quality of the Pareto sets generated by the considered algorithms.

ICCS Camera Ready Version 2026
To cite this paper please use the final published version:
DOI: 10.1007/978-3-032-29921-5_25

3.1 Test Problems

The test antennas are shown in Fig. 6. The first device is a broadband monopole, whereas the second is a quasi-Yagi structure. Figure 7 provides data on antenna substrates and decision variables. Figure 8 incorporates essential information concerning design objectives and parameter spaces (the lower and upper parameter bounds $\boldsymbol{l}$ and $\boldsymbol{u}$). The design goals for Antenna I are size reduction (objective F_1), and to in-band impedance matching improvement (objective F_2). Antenna II is designed to maximize the end-fire realized gain (objective F_1), and to enhance the in-band reflection coefficient (objective F_2).

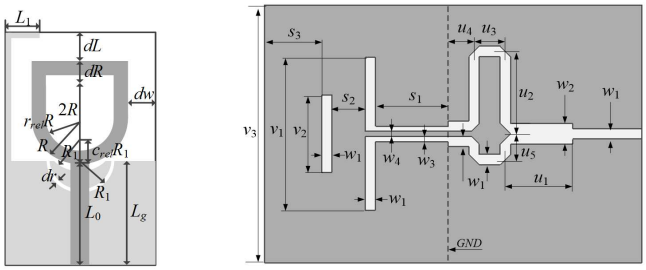

(a) (b)

Fig. 6. Verification structures: (a) Antenna I, (b) Antenna II.

Antenna	Substrate	Designable parameters [mm]	Other parameters [mm]
I [36]	RF-35 (ε_r = 3.5, h = 0.762 mm)	$\boldsymbol{x}$ = [L_0 dR R r_{rel} dL dw Lg L_1 R_1 dr c_{rel}]^T	w_0 = 1.7
II [37]	RT6010 (ε_r = 10.2, h = 0.635 mm)	$\boldsymbol{x}$ = [s_1 s_2 v_1 v_2 u_1 u_2 u_3 u_4]^T	w_1 = w_3 = w_4 = 0.6, w_2 = 1.2, u_5 = 1.5, s_3 = 3.0 and v_3 = 17.5

Fig. 7. Parameters of Antenna I and II.

Antenna	Design goals		Parameter space
	Objective F_1	Objective F_2	
I	Minimize antenna footprint area: $F_1(\boldsymbol{x}) = A(\boldsymbol{x})$ (unit: mm^2)	Minimize maximum in-band reflection within the UWB band (3.1 to 10.6 GHz): $F_2(\boldsymbol{x}) = \max\{f \in [3.1\ 10.6]\ \text{GHz} : \lvert S_{11}(\boldsymbol{x},f)\rvert\}$	$\boldsymbol{l}$ = [8.0 0.0 4.0 0.1 0.0 1.2 9.0 4.0 2.0 0.5 0.2]^T $\boldsymbol{u}$ = [11.0 2.0 6.0 0.75 4.0 6.2 10.5 6.0 3.0 1.0 0.9]^T
II	Maximize average in-band end-fire gain within the frequency range F from 10 GHz to 11 GHz: $F_2(\boldsymbol{x}) = -\lvert F\rvert^{-1}\int_{f\in F} G(\boldsymbol{x},f)df$	Minimize maximum in-band $\lvert S_{11}\rvert$ within the frequency range from 10 to 11 GHz: $F_2(\boldsymbol{x}) = \max\{f \in [10\ 11]\ \text{GHz} : \lvert S_{11}(\boldsymbol{x},f)\rvert\}$	$\boldsymbol{l}$ = [4.4 3.8 7.0 4.2 3.5 4.7 2.0 0.9]^T $\boldsymbol{u}$ = [5.3 7.0 8.9 5.2 4.2 5.0 2.3 1.7]^T

Explanation of symbols: $|S_{11}(\boldsymbol{x},f)|$ - reflection at design $\boldsymbol{x}$ and frequency f; $G(\boldsymbol{x},f)$ – end-fire gain at design $\boldsymbol{x}$ and frequency f.

Fig. 8. Design goals and search spaces for Antennas I and II.

ICCS Camera Ready Version 2026
To cite this paper please use the final published version:
DOI: 10.1007/978-3-032-29921-5_25

3.2 Setup and Benchmark Methods

The test antennas are optimized using the algorithm described in Section 2 with default control parameter settings. The result of the MO process is a Pareto set incorporating non-dominated designs identified from the EM-evaluated set $\{\boldsymbol{x}_T^{(i,j)}\}$ generated during the optimization run.

Our method is compared to three surrogate-based MO techniques, illustrated in Fig. 9. Algorithms 1 and 2 are off-line approaches, where the surrogate is constructed in advance and then optimized using MOEA. In Algorithm 1, the metamodel is built using kriging interpolation, whereas Algorithm 2 employs a multi-layer perceptron ANN. Each procedure is executed in two variants: (i) a surrogate trained with $N = 400$ samples (Version 1), and (ii) a surrogate trained with $N = 1600$ (Version 2). The third benchmark (Algorithm 3) resembles our proposed framework but omits the intermittent local design refinement. This comparison highlights the benefits of the algorithmic enhancements introduced in this work.

3.3 Results and Summary of Findings

The results produced by the presented framework and the benchmark techniques are summarized in Table 2 and illustrated in Figs. 10 and 11. The comparison focuses on the MO cost and the visual inspection of the Pareto sets produced by all methods. Additionally, Figs. 10 and 11 visualize antenna responses at selected Pareto-optimal designs obtained with our approach. It is important to emphasize that the costs reported in Table 1 account solely for EM simulations. Other expenses, such as surrogate training or MOEA-based optimization of the metamodel, are negligible. For instance, ANN training requires only about twenty seconds due to the simplicity of the network architecture, whereas a single EM simulation takes between two and seven minutes, depending on the antenna and parameter vector under consideration.

Algorithm	Characterization
Algorithm 1	• One-shot surrogate-assisted MO procedure; • Surrogate model: kriging interpolation with Gaussian correlation functions and first-order polynomial as a trend function; • Surrogate constructed using N_S data samples, then optimized using MOEA; • Selected non-dominated samples evaluated with EM analysis to form the final outcome of the algorithm.
Algorithm 2	• One-shot surrogate-assisted MO procedure; • Surrogate model: neural network (setup: multi-layer perceptron, two hidden layers, ten neurons each; training: Levenberg-Marquardt algorithm); • Surrogate constructed using N_S data samples, then optimized using MOEA; • Selected non-dominated samples evaluated with EM analysis to form the final outcome of the algorithm.
Algorithm 3	• Machine learning algorithm with ANN surrogates; • Initial sampling and surrogate model setup the same as discussed in Section 2.3; • Infill point generation as discussed in Section 2.4 and 2.5 (surrogate optimization using MOEA); • EM-simulation dataset updates by adding all infill points to the existing dataset; • The search process executed using a single (high-fidelity) EM simulation model.

Fig. 9. Benchmark techniques: the outline.

ICCS Camera Ready Version 2026
To cite this paper please use the final published version:
DOI: 10.1007/978-3-032-29921-5_25

Table 2. The MO cost of the proposed machine learning procedure with local design enhancement and the benchmark routines

Algorithm		Optimization cost#	
		Antenna I	Antenna II
This work (ML with ANN surrogates and local design enhancement)		260	300
Algorithm 1	N = 400	400	400
	N = 1600	1600	1600
Algorithm 2	N = 400	400	400
	N = 1600	1600	1600
Algorithm 3		320	340

#Cost expressed in the number of EM simulations of the antenna under design. Other expenses (surrogate model construction, model optimization, etc., are negligible compared to EM analysis).

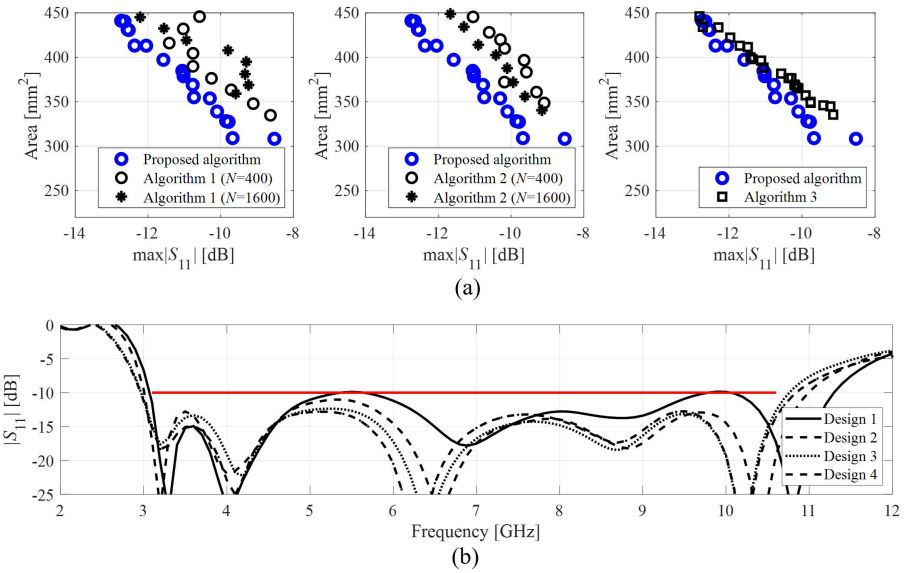

Fig. 10. Multi-objective optimization results for Antenna I generated using the suggested MO framework and the benchmark: (a) Pareto sets obtained with our algorithm vs. Algorithms 1, 2, and 3; (b) $|S_{11}|$ at selected Pareto-optimal designs produced using our algorithm: Design 1 (A = 328 mm^2), Design 2 (A = 379 mm^2), Design 3 (A = 413 mm^2), Design 4 (A = 442 mm^2).

As shown in Figs. 10 and 11, the proposed MO procedure consistently outperforms all benchmark algorithms in terms of reliability. The Pareto sets generated by our method are markedly better than those obtained with Algorithms 1 and 2, primarily due to the inferior predictive power of the underlying surrogates. For instance, with N = 400 training samples, the relative RMS error reaches approximately 20% (Antenna I) and 8% (Antenna II). Increasing the training set to N = 1600 improves surrogate accuracy (to about 15% and 6% RMS error, respectively), which results in higher-quality Pareto fronts, yet still inferior to those generated by our technique. The differences with Algorithm 3 are less pronounced; however, our method still produces consistently better

ICCS Camera Ready Version 2026
To cite this paper please use the final published version:
DOI: 10.1007/978-3-032-29921-5_25

Pareto sets, except for Antenna II, where both approaches perform comparably. These findings highlight the general advantage of machine learning over offline surrogate-assisted optimization. ML-based frameworks allow the search process—and surrogate refinement—to be concentrated within the promising parameter space areas, thereby enhancing predictive accuracy as optimization progresses. Importantly, the high design quality achieved by our methodology underscores the added value of the local enhancement mechanism integrated into the algorithm.

The advantages of the proposed approach analyzed through visual inspection of Pareto sets is corroborated by quantitative performance metrics, in particular the hypervolume indicator (computed for normalized objectives). For Antenna I, the hypervolume values are 0.16, 0.19, 0.14, and 0.18 (Algorithm 1 with $N = 400$ and 1600 samples, and Algorithm 2 with $N = 400$ and 1600 samples), 0.31 (Algorithm 2), and 0.32 (proposed procedure). For Antenna II, the numbers are 0.41, 0.40, 0.40, 0.39 (Algorithms 1 and 2), 0.44 (Algorithm 3), and 0.45 (proposed technique).

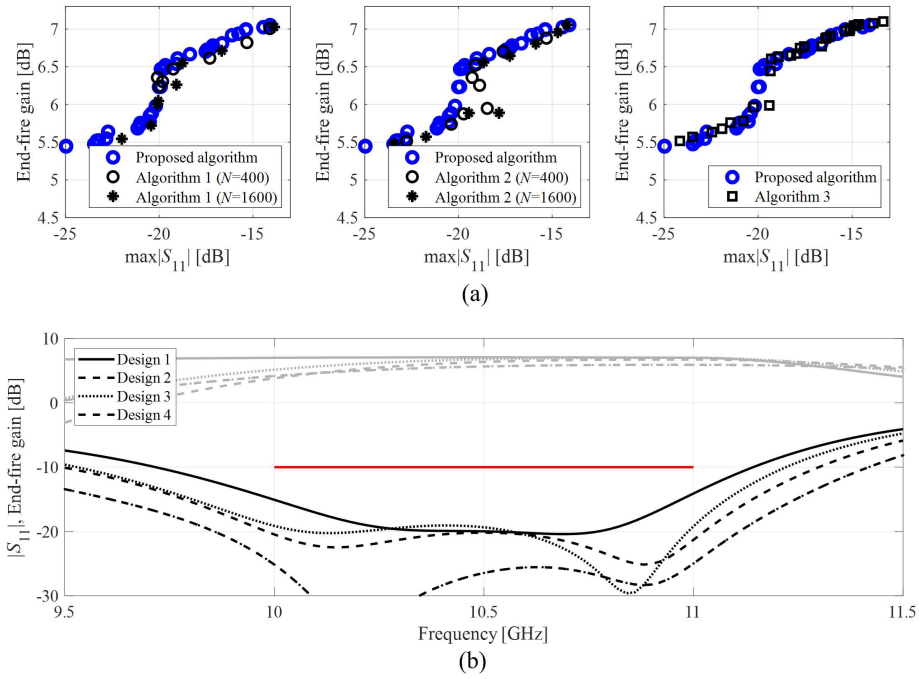

Fig. 11. Multi-objective optimization results for Antenna II generated using the suggested MO framework and the benchmark: (a) Pareto sets obtained with our algorithm versus Algorithms 1, 2, and 3; (b) $|S_{11}|$ (black) and end-fire gain (gray) at selected Pareto-optimal designs obtained using our algorithm: Design 1 (gain = 7.1 dB), Design 2 (gain = 6.5 dB), Design 3 (gain = 6.0 dB), Design 4 (gain = 5.4 dB).

ICCS Camera Ready Version 2026
To cite this paper please use the final published version:
DOI: 10.1007/978-3-032-29921-5_25

The cost analysis summarized in Table 2 shows that the reliability improvements offered by the proposed methodology are not achieved at the expense of computational efficiency. On the contrary, incorporating the local refinement step substantially accelerates convergence, despite each iteration being twice as expensive as in Algorithm 3 (requiring $2N_{infill}$ EM simulations versus N_{infill}). The average total cost of our procedure amounts to only 280 EM evaluations, translating into more than 80% savings compared to Algorithms 1 and 2 (Version II with $N = 1600$ training samples). A further advantage is a nearly 20% speedup relative to Algorithm 3.

Overall, the proposed framework demonstrates an advantageous balance of reliability, computational efficiency, and ease of implementation, establishing it as a compelling alternative to multi-objective optimization methods reported in the literature to date.

4 Conclusion

In this paper, we presented a novel technique for cost-efficient and dependable multi-objective optimization of antennas. Our framework integrates ML with ANN surrogates and intermittent local refinement. In each iteration, multiple candidate Pareto-optimal solutions are generated using ANN predictions optimized via a multi-objective evolutionary algorithm. These designs are subsequently refined through a single trust-region, gradient-based adjustment, with response sensitivities estimated from the surrogate. This mechanism accelerates convergence, reduces computational cost, and yields higher-quality Pareto sets compared with conventional ML-based methods.

The presented approach was verified using two planar antennas optimized for minimum footprint, impedance matching, and gain improvement. Extensive comparisons with diverse surrogate-assisted methods confirm its exquisite performance regarding Pareto set quality and computational efficiency. The proposed approach delivers relative acceleration of about 20% over multi-point ML algorithms and up to 80% over offline methods. Additional benefits include straightforward implementation and minimal problem-dependent parameterization. Future work will address further improvements in efficiency and extend applicability to higher-dimensional tasks, including the incorporation of dimensionality reduction strategies.

Acknowledgement

The authors would like to thank Dassault Systemes, France, for making CST Microwave Studio available. This work is partially supported by the Icelandic Research Fund Grant 239858 and by National Science Centre of Poland Grant 2022/47/B/ST7/00072.

References

1. Vinnakota, S.S., Kumari, R., Majumder, B., Metasurface-assisted broadband compact dual-polarized dipole antenna for RF energy harvesting. *IEEE Ant. Wireless Propag. Lett.*, **22**, 1912–1916 (2023)

ICCS Camera Ready Version 2026
To cite this paper please use the final published version:
DOI: 10.1007/978-3-032-29921-5_25

2. Cho, H., Lee, J.-H., Yu, J.-W., Ahn, B., Series-fed coupled split-ring resonator array antenna with wide fan-beam and low sidelobe level for millimeter-wave automotive radar. *IEEE Trans. Vehicular Techn*., **72**, 4805–4814 (2023)
3. Li, M., Yang, Z., Zhang, Z., Tang, M.-C., Zhu, L. Miniaturized slow-wave transmission line-based annular ring antenna with reconfigurable circular polarization and high gain. *IEEE Ant. Wireless Propag. Lett.*, **22**, 1766–1770 (2023)
4. Singh, M., Parihar, M.S., Gain improvement of Vivaldi MIMO antenna with pattern diversity using bi-axial anisotropic metasurface for millimeter-wave band application, *IEEE Ant. Wireless Propag. Lett.*, **22**, 621–625 (2023)
5. Fan, F.-F., Chen, Q.-L., Xu, Y.-X., Zhao, X.-F., Feng, J.-C., Yan, Z.H. A wideband compact printed dipole antenna array with SICL feeding network for 5G application. *IEEE Ant. Wireless Propag. Lett.*, **22**, 283–287 (2023)
6. Esmail, B.A.F., Koziel, S., Design and optimization of metamaterial-based dual-band 28/38 GHz 5G MIMO antenna with modified ground for isolation and bandwidth improvement. *IEEE Ant. Wireless Propag. Lett.*, **22**, 1069–1073 (2023)
7. Huang, Y.-S., Zhou, L., Xu, Q.-H., Mao, J.-F., A W-band self-packaged SIW-based slot antenna with gain and bandwidth enhancement. *IEEE Trans. Ant. Propag.*, **71**, 2158–2166 (2023)
8. Lu, W. *et al.*, Design of microwave ablation antenna for flexible omnidirectional/directional ablation zone control. *IEEE Ant. Wireless Prop. Lett.*, **24**, 18–22 (2025)
9. Koziel, S., Pietrenko-Dabrowska, A., Recent advances in accelerated multi-objective design of high-frequency structures using knowledge-based constrained modeling approach. *Knowledge Based Syst*., **214**, paper no. 106726 (2021)
10. Koziel, S., Pietrenko-Dabrowska, A., Constrained multi-objective optimization of compact microwave circuits by design triangulation and Pareto front interpolation. *European J. Op. Research*, **299**, 302–312 (2022)
11. Koziel, S., Pietrenko-Dabrowska, A., Tolerance-aware multi-objective optimization of antennas by means of feature-based regression surrogates. *IEEE Trans. Ant. Propag.*, **70**, 5636–5646 (2022)
12. Marler, T. Arora, J.S., Multi-Objective Optimization: Concepts and Methods for Engineering, VDM Verlag (2009)
13. Lei, S., Chen, B., Lin, Z., Yang, W., Tian, J., Hu, H. Sidelobe-level minimization with power gain constraint via a wide-beam antenna array. *IEEE Ant. Wireless Propag. Lett.*, **22**, 422–426 (2023)
14. Zhang, J., Xu, J., Chen, Q., Li, H. Machine-learning-assisted antenna optimization with data augmentation, *IEEE Ant. Wireless Propag. Lett.*, **22**, 1932–1936 (2023)
15. Mirjalili, S., Dong, J.S., Multi-Objective Optimization using Artificial Intelligence Techniques, Springer Briefs in Applied Sciences and Technology, New York, (2019)
16. Fan, M., Chen, J., , Z., Xie, Li, S., Gao, L., Improved multi-objective differential evolution algorithm based on a decomposition strategy for multi-objective optimization problems, *Sc. Rep.*, **12**, paper no. 21176 (2022)
17. Yang, Y., Liao, Q., Wang, J., Wang, Y., Application of multi-objective particle swarm optimization based on short-term memory and K-means clustering in mjulti-modal multi-objective optimization, *Eng. Appl. Art. Intelligence*., **112**, paper no. 104866 (2024)
18. Zeng, Y., Qing, X., Chia, M.Y.W., A wideband circularly polarized antenna with a nonuniform metasurface designed via multiobjective Bayesian optimization. *IEEE Ant. Wireless Propag. Lett.*, **23**, 1739–1743 (2024)

ICCS Camera Ready Version 2026
To cite this paper please use the final published version:
DOI: 10.1007/978-3-032-29921-5_25

19. Wu, Q., Chen, W., Yu, C., Wang, H., Hong, W. Machine-learning-assisted optimization for antenna geometry design. *IEEE Trans. Ant. Propag.*, **72**, 2083–2095 (2024)
20. Koziel, S., Pietrenko-Dabrowska, A., Efficient simulation-based global antenna optimization using characteristic point method and nature-inspired metaheuristics. *IEEE Trans. Ant. Propag.*, **72**, 3706–3717 (2024)
21. He, Y., Huang, J., Li, W., Zhang, L., Wong, S.W., Chen, Z.N., Hybrid method of artificial neural network and simulated annealing algorithm for optimizing wideband patch antennas. *IEEE Trans. Ant. Propag.*, **72**, 944–949 (2024)
22. Wang, X., Wang, G., Wang, D., Zhang, Q., Ensemble-learning-based multiobjective optimization for antenna design. *IEEE Trans. Ant. Propag.*, **71**, 1295–1303 (2023)
23. Xiao, S., Liu, G.Q., Zhang, K.L., Jing, Y.Z., Duan, J.H., Di Barba, P., Sykulski, J.K., Multiobjective Pareto optimization of electromagnetic devices exploiting kriging with Lipschitzian optimized expected improvement, *IEEE Trans. Magn.*, **54**, paper no. 7001704 (2018)
24. Unnsteinsson, S.D., Koziel, S., Generalized Pareto ranking bisection for computationally feasible multi-objective antenna optimization. *Int. J. RF & Microwave Eng.*, **28**, 8 (2018)
25. Koziel, S., Pietrenko-Dabrowska, A., Performance-driven surrogate modeling of high-frequency structures, Springer, New York, (2020)
26. Koziel, S., Pietrenko-Dabrowska, A., Leifsson L. Improved efficacy behavioral modeling of microwave circuits through dimensionality reduction and fast global sensitivity analysis. *Sc. Rep.*, **14**, paper no. 19465 (2024)
27. Koziel, S., Pietrenko-Dabrowska, A., Constrained multi-objective optimization of compact microwave circuits by design triangulation and Pareto front interpolation. *European J. Op. Research*., **299**, 302–312 (2022)
28. Deb, K., *Multi-Objective Optimization Using Evolutionary Algorithms.* Wiley, New York (2001)
29. Zhang, C., Fu, X., Chen, X., Peng, S., Min, X., Synthesis of uniformly excited sparse rectangular planar array for sidelobe suppression using multi-objective optimization algorithm, *J. Eng.*, **2019**, 6278–6281 (2019)
30. Hasbestan, V. H., Farhang, Y., Majidzadeh, K., Ghobadi, C., Multi-objective hybrid optimization algorithm for design a printed MIMO antenna with n78–5G NR frequency band applications, *IEEE Access*, **11**, 68231–68242 (2023)
31. Sarker, N., Podder, P., Mondal, M. R. H., Shafin, S. S., Kamruzzaman, J., Applications of machine learning and deep learning in antenna design, optimization, and selection: a review, *IEEE Access*, **11**, 103890–103915 (2023)
32. Vang-Mata, R. (Ed.), *Multilayer perceptrons*, Nova Science Pub. Inc. (2020)
33. Beachkofski, B., Grandhi, R., Improved distributed hypercube sampling, *American Institute of Aeronautics and Astronautics*, paper AIAA 2002-1274 (2002)
34. Fonseca, C.M., Fleming, P.J., Multiobjective optimization and multiple constraint handling with evolutionary algorithms–Part I: a unified formulation, *IEEE Trans. Syst. Man Cybernetics: Part A: Syst. Humans*, **28**, 26–37 (1998)
35. Conn, A.R., Gould, N.I.M., Toint, P.L., *Trust Region Methods*, MPS-SIAM Series on Optimization (2000)
36. Alsath, M.G.N., Kanagasabai, M., Compact UWB monopole antenna for automotive communications, *IEEE Trans. Ant. Prop.*, **63**, 9, 4204–4208 (2015)
37. Kaneda, N., Deal, W.R., Qian, Y., Waterhouse, R., Itoh, T., A broad-band planar quasi Yagi antenna, *IEEE Trans. Antennas Propag.*, **50**, 1158–1160 (2002)

ICCS Camera Ready Version 2026
To cite this paper please use the final published version:
DOI: 10.1007/978-3-032-29921-5_25